Silver-polymethylhydrosiloxane nanocomposite coating on anodized aluminum with superhydrophobic and antibacterial properties

Henry Agbe[1], Dilip Kumar Sarkar[1*], X.-Grant Chen[1], Nathalie Faucheux[2] ,Gervais Soucy[2], Jean-Luc. Bernier[3]

[1] Department of Applied Science, University of Québec at Chicoutimi, Aluminum Research Center – REGAL, Chicoutimi, QC, Canada, G7H 2B1.

[2] Department of Chemical and Biotechnological Engineering, Université de Sherbrooke, Sherbrooke, QC, Canada, J1K2R1

[3] A3 Surfaces, Chicoutimi, QC, Canada, G7H 1Z6.

KEYWORDS: Ag nanocomposite; anodized aluminum; superhydrophobic coating; antibacterial properties; anti-biofouling surface.

ABSTRACT:

Biofilm formation on both animate and inanimate surfaces serves as an ideal bacterial reservoir for the spread of nosocomial infections. Designing surfaces with both superhydrophobic and antibacterial properties can help reduce initial bacterial attachment and subsequent biofilm formation. In the present study, a two-step approach is deployed to fabricate silver-polymethylhydrosiloxane (Ag-PMHS) nanocomposites, followed by a simple dip-coating deposition on anodized Al. Ag-nanoparticles (Ag-NPs) are synthesized in-situ within a PMHS polymeric matrix. Morphological features of Ag-PMHS coating observed by scanning electron

microscopy shows heterogeneous micro–nano structures. The chemical compositions of these coatings were characterized using X-ray diffraction and attenuated total reflection-Fourier Transform infrared spectroscopy, which indicate the presence of a low-energy PMHS polymer.

The as-synthesized Ag-PMHS nanocomposite demonstrated excellent antibacterial properties against clinically relevant planktonic bacteria, with zone of inhibition values of 25.3 ± 0.5, 24.8 ± 0.5, and 23.3 ± 3.6 mm for *Pseudomonas aeruginosa* (P.A) (gram -ve), *Escherichia coli* (E-coli) (gram -ve), and *Staphylococcus aureus* (S.A) (gram +ve), respectively. The Ag-PMHS nanocomposite coating on anodized Al provides an anti-biofouling property with an adhesion reduction of 99.0 %, 99.5 %, and 99.3 % for *Pseudomomas aeruginosa* (P.A), *Escherichia-Coli* (E-coli) and *Staphyloccocus aureus (*S.A), respectively. Interestingly, the coating maintained a stable contact angle of 158° after 90 days of immersion in saline water (3.5 wt.% NaCl, pH = 7.4).

The Ag-PMHS nanocomposite coating on anodized Al described herein demonstrates excellent antibacterial and anti-biofouling properties, owing to its inherent superhydrophobic property

INTRODUCTION

Bacteria colonize material surfaces and develop into a community (in extracellular polymeric substance (EPS) matrix), herein referred to as a biofilm [1]. The pathogenicity of bacteria in a biofilm differs from their free-floating planktonic cells. A biofilm offers bacteria certain advantages such as the ability to acquire resistant strains [2], intercellular communication ability to regulate gene expression via quorum sensing (QS) [3], and the ability to evade antimicrobial attacks[4]. Furthermore,

a biofilm provides a safe haven for the spread of nosocomial infections [5]. It is believed that multidrug-resistant (MDR) bacteria in biofilms (*Staphyloccocus aureus* (S.A)*, Pseudomomas aeruginosa* (P.A), *and Escherichia-Coli* (E-coli)) are the leading cause of nosocomial infections or heathcare-associated infections [6-7]. Therefore, designing anti-biofouling surfaces for preventing initial bacterial attachment and subsequent biofilm formation using superhydrophobic coatings has recently gained significant interest [8-10]. However, the ability of superhydrophobic coatings to repel bacterial adhesion in humid environments is limited, mainly due to the loss of property of water repellency[11-14]. To achieve a robust and long-term anti-biofouling surface, it is desirable to incorporate bactericides such as Ag. Hence, fabricating superhydrophobic coatings with inherent antibacterial properties may serve as an ideal strategy to prevent initial bacterial adhesion and subsequent biofilm formation.

Few studies have reported the fabrication of anti-biofouling surfaces (utilizing superhydrophobicity) with inherent antibacterial properties [15-17]. Wang, Z. et al. [17] fabricated mussel-inspired polydopamine superhydrophobic Ag coatings via a facile Ag mirror reaction and evaluated both the antibacterial and superhydrophobic properties against S.A and E-coli. They demonstrated that the superhydrophobic Ag coating exhibited antibacterial properties with a zone of inhibition (ZOI) of ~3.0 ± 0.3 mm and stability of 60 days. Meanwhile, Zhang, M. et al. [15] fabricated a Ag/Cu bimetallic hierarchical architecture coating on a copper substrate with both superhydrophobic and antibacterial properties using a facile galvanic replacement reaction, followed by a simple thermal oxidation process. The study indicated both antibacterial and superhydrophobic properties but failed to report the anti-biofouling property. Furthermore, Ozkan, E. et al. [18] engineered a superhydrophobic antibacterial copper coating via aerosol-assisted chemical vapor deposition (AACVD) with antibacterial properties against E. coli and S.A. Even

though the superhydrophobic coatings of these studies were well above 150° in contact angle (CA), the antibacterial efficiency was low. Moreover, synthesis methods such as AACVD are expensive. For practical applications, a simple, cost-effective, and scalable process would be the sol–gel synthesis of superhydrophobic Ag nanocomposite coatings on metals such as Al.

It has been reported that polymethylhydrosiloxane (PHMS) can be utilized to synthesize silver nanoparticles (Ag-NPs) via the sol–gel process owing to its ability to reduce Ag^{+} to Ag^{0} in-situ, due to the (Si–H) moiety on the siloxane backbone [19-20]. Several groups have explored the synthesis of Ag-NPs via PMHS reduction [19-22]. For example, Shang, R. et al. [21], reported the synthesis of an Ag-NP-embedded PMHS hybrid material with high surface area, good mesoporosity, and narrow size distribution. Similarly, Zuo,Y. et al. [19] synthesized hollow Ag–SiO_2 composite spheres that exhibited high catalytic performance. Additionally, our research group has recently fabricated superhydrophobic coatings on Al using a TiO_2/PMHS sol–gel process.

In spite of significant efforts on silicone-based superhydrophobic coatings in applications of antibacterial properties, the adhesion reduction performance of bacteria has been rather low (79 - 95 %)[23-24]. Furthermore, the applicability of such coating is limited due to the degradation with time. As Ag has natural properties to kill bacteria, incorporating it in silicone-based superhydrophobic coatings such as polymeric PMHS could reduce the bacterial adhesion (anti-biofouling) and improve the overall longevity of such coatings even after the loss of superhydrophobicity. Surprisingly, fabrication of superhydrophobic Ag-PMHS nano-composite coatings with inherent antibacterial and anti-biofouling properties is yet to be reported in the literature.

The objective of this study is to fabricate a novel coating of Ag-PMHS nanocomposites on anodized Al via the sol–gel process for antibacterial and anti-biofouling applications. We hypothesize that the in-situ synthesis of Ag-NPs within a PMHS polymeric matrix, anchored within an anodized Al oxide (AAO) substrate, could enhance the adhesion, durability, and stability of superhydrophobic Ag-PMHS nanocomposites. PMHS not only serves as a reducing agent, but also a morphological controlling agent for holding and presumably triggering controllable Ag^+ release. The excellent antibacterial and antibiofouling properties, owing to the inherent superhydrophobicity of the Ag-PMHS nanocomposite coating on anodized Al, are demonstrated.

MATERIALS AND METHODS

Synthesis of Ag–PMHS nanocomposite. Ethanoic polymethylhydrosiloxane (PMHS) (≥ 97%, VWR) stock solution was sonicated (Branson® Ultrasonic Bath, 230 Vac, 50 Hz) for 15 min for dispersion. Subsequently, 0.08 M PMHS was added to mineral spirit while stirring using a magnetic Teflon stirrer rotating at 500 rpm at 55 °C for 30 min. Next, Ammonium hydroxide 11.2 M (28 – 30 wt.% of NH_3,-VWR) was added dropwise to the suspension to achieve a pH of 11. The sol–gel reaction was allowed to age briefly for 30 min. Subsequently, 0.08 M $AgNO_3$ (VWR) solution was added dropwise to the above suspension according to the Ag^+/Si–H molar ratio (Table 1). The as-synthesized product was stirred vigorously using a magnetic Teflon stirrer rotating at 700 rpm at 55 °C for an additional 15 min.

Table 1: Ag-PMHS molar ratio.

Samples	Ag^{+}/Si-H molar ratio	Volume of Mineral Spirit (mL)
1	50:1	15
2	50: 2	15
3	50:30	15
4	50: 40	15
5	50:50	15
6	2: 50	15
7	1 :50	15

Fabrication of Ag-PMHS nanocomposite coating on AAO substrates. The as-synthesized Ag-PMHS nanocomposite was loaded with premium room-temperature vulcanized (RTV) adhesive silicone. The RTV silicone (0.0 % (w/v), 0.4 % (w/v), 2.0 % (w/v), 4.0 % (w/v), 6.0 % (w/v), and 8.0 % (w/v))-loaded Ag-PMHS nanocomposite was sonicated to obtain a homogeneous dispersion. The Ag-PMHS polymeric solution above was coated on an AAO substrate through a 5-min dip coating deposition process, followed by room-temperature drying for 24 h. The anodization process was performed as follows: A 1″ × 2″ Al (AA6061) was ultrasonically degreased in a soapy solution and cleaned in deionized water, followed by 1 M NaOH (VWR) chemical etching at 55 °C to remove a superficial oxide layer. Then the etched substrate was further sonicated in

distilled water. Afterward, etched Al substrate was subsequently immersed in HNO_3 solution (10 wt.%, VWR) for desmutting, followed by rinsing in distilled water. Next, both etched-and as-received Al substrates were used as anode and cathode, respectively. The electrochemical cell was equipped with a 600 W direct current power supply (Ametek Sorensen DCS 100-12E, Chicoutimi, QC, Canada), a quartz-jacketed beaker with cold circulating water (5 °C), and a small magnetic Teflon stirrer, rotating at 2000 rpm. Anodization was performed in the galvanostatic mode at a current density of 40 mA/cm^2 and electrolyte concentration of (H_2SO_4 -15 wt.%,-VWR), with varying times of 30, 60, and 120 min. During anodization, the two electrodes were separated in parallel by a distance of 1.5 cm. For quality control and reproducibility, each experiment was triplicated.

Sample characterization. The surface morphology and elemental analysis of the Ag-PMHS nanocomposite were performed using scanning electron microscopy (SEM, JEOL JSM-6480 LV), equipped with energy dispersive X-ray spectroscopy (EDX). The crystalline structure and chemical composition of the synthesized Ag-PMHS nanocomposite were analyzed with X-ray powder diffraction (XRD) (a Bruker D8 Discover system) and attenuated total reflection-Fourier transform infrared (ATR-FTIR, Perking Elmer Spectrum One), respectively. Static CA was measured with a First Ten Angstorm CA goniometer using 10 µL of deionized water drops. The roughness of the Ag-PMHS nanocomposite coating on anodized Al was measured using a MicroXAM-100 HR 3D surface profilometer.

Antibacterial susceptibility assay. The model bacterial strain, i.e., S.A (ATCC 6538), P.A (ATCC 9027), and E-coli (ATCC 8739-Hardy Diagnostics) were grown overnight from a frozen

(-80 °C) stock in tryptic soy broth (TSB-Hardy Diagnostics) at 37 °C, re-inoculated in fresh TSB (37 °C), and grown to 10^8 colony forming units (CFU)/mL, as determined by their optical density at 625 nm and verified by both replicate plating on nutrient agar [25] and the 0.5 McFarland standard. An antibacterial assay was studied using the Kirby Bauer disk diffusion assay on S.A (gram +ve), P.A. (gram -ve), and E-Coli (gram -ve)[26]. Briefly, bacteria were inoculated in physiological saline (0.85% wt NaCl-Sigma–Aldrich). Sterile swab was used to inoculate isolates over the agar surface, followed by streaking to obtain a bacterial lawn. Next, 5 µL of Ag-PMHS nanocomposite was carefully seeded onto a 6 mm agar disk. Finally, the plates were aerobically incubated at 37 °C for 24 h in an incubator. Subsequently, the results were analyzed by measuring the ZOI. Three independent experiments were triplicated. Data were analyzed by a one-way analysis of variance (ANOVA) with the Tukey–Kramer multiple comparison test. Results were considered significant at $p < 0.05$.

Anti-biofouling and biofilm inhibition assay. Bacterial strain was grown overnight to obtain 10^8 CFU/mL. Anti-biofouling experiment was conducted using a protocol described elsewhere [23] with minor modifications. Briefly, two staining jars were filled with 99 mL physiological saline (0.85% wt NaCl) and 1 mL bacterial culture. Subsequently, both 2.54 cm × 2.54 cm anodized Al (Al/AAO, used as control) and superhydrophobic AAO/Al sample (04Sil-AgP-NcAAO), were placed in two separate jars. The staining jars were incubated for 3 h at 37 °C. The substrates were subsequently removed and gently immersed in physiological saline to rinse non-adherent bacteria. Next, the substrates were transferred into a set of 80 mL sterile beakers containing physiological saline and sonicated on ice for 10 min to remove adherent bacteria. Finally, the bacterial suspensions were serially diluted and then plated on tryptic soy agar, followed by an aerobic incubation at 37 °C for

24 h. Positive controls were performed for t = 0 and t = 3 h to ascertain the bacterial viability. Three independent experiments were performed in triplicate to determine the number of adherent bacteria. Relative bacterial adhesion reduction was calculated using the following formula: Relative bacterial adhesion reduction = [(A-B)/A×100 %], where A = CFU/cm^2 of adherent bacteria on anodized Al (AAO/Al) and B = CFU/cm^2 of adherent bacteria on superhydrophobic AAO/Al sample (04Sil-AgP-NcAAO). Biofilm inhibition study was also performed on E-coli bacterium for 48 h to evaluate the ability of superhydrophobic AAO/Al sample (04Sil-AgP-NcAAO) at inhibiting E-coli bacterium colonization. Test culture was diluted with physiological saline (0.85% wt. NaCl) (Sigma–Aldrich) to achieve a bacterial inoculum concentration of 1.0 × 10^7 colony-forming units/millilitre (CFU) mL^{-1} . Next, 22.5 mL tryptic soy broth was added to 2.5 mL bacterial inoculum in separate sterile petri dishes. Both the test sample (04Sil-AgP-NcAAO) and the control sample (AAO/Al) were then immersed in these petri dishes, followed by 48 h incubation for biofilm growth. Subsequently, samples were rinsed with the physiological saline, followed by air-drying in airflow Class II cabinet at ambient conditions of 25 °C and (50 ± 10 %) relative humidity (RH) for 1 h. Samples were finally metalized with gold coating and imaged in a high vacuum SEM. Data were analyzed by ANOVA with the Tukey–Kramer multiple comparison test. Results were considered significant at $p < 0.05$.

RESULTS AND DISCUSSION

Synthesis of Ag–PMHS nanocomposites. PMHS is a linear organofunctional polysiloxane, in which the active moiety, (Si–H) reacts with metallic salts to form the corresponding metallic

particles owing to the strong reducing ability of the PMHS [19]. In particular, when silver salts such as $AgNO_3$ react with the PMHS, the Si–H bond is oxidized into Si–O–Si species with H_2 gas evolution and hydridic hydrogen replaced by Ag-NPs [20] as seen in Eq. 1.

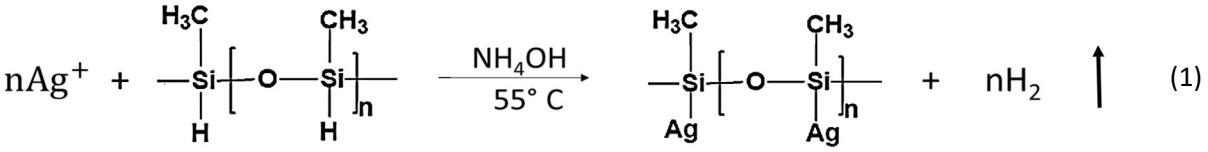

(1)

The polymeric PMHS matrix is an ideal template for in-situ Ag-NPs synthesis, similar to the typical host–guest redox reaction [19]. It is noteworthy that such a host–guest structure might exhibit interesting antibacterial properties, in which PMHS acts as a polymeric matrix for holding and presumably triggering controllable Ag^+ release for killing or inhibiting bacterial growth.

To ascertain the amount of Ag^+ ions required to react with the active Si–H moiety, the Ag^+/Si–H molar ratio was varied from 1:50 to 50:1 (Table 1). Figure 1 shows the ATR-FTIR spectra of PMHS before and after reaction with $AgNO_3$ for different molar ratios of Ag^+/Si–H. Figure 1 (III) shows the ATR-FTIR spectrum of liquid PMHS. The single peak at 2939 cm^{-1} at the high-frequency region can be assigned to the asymmetric stretching mode of $-CH_3$ groups in the PMHS molecule [27]. At the lower frequency region, the two peaks at 1270 and 764 cm^{-1} correspond to $Si-CH_3$ groups [28]. Similarly, the peak at 1100 cm^{-1} can be linked to the asymmetrical stretching vibration of the Si−O−Si mode [29], while that around 800 cm^{-1} can be attributed to the symmetric bending mode of the Si–O–Si bonds [30]. The peak at 2162 cm^{-1} at the mid-frequency region is assigned to the Si−H stretching mode. Notably, at a lower molar ratio of Ag^+/Si–H , such as 2:50 (Figure 1.(II)), the intensity of the Si–H group marginally decreases by ~10 % compared with the

as-received PMHS, suggesting that less amount of Si−H species are consumed. However, at higher molar ratios of Ag^+/Si–H such as 50:2, the Si−H group is no longer observed (Figure 1 (I)), signifying that all the Si−H species are consumed. A similar observation was made by Omer D. et al. [20], however, their Si–H peak intensity at a higher Ag^+/Si-H molar ratio (1:1) decreased by 90 % compared with ours of 100 %, owing to the total consumption of the Si–H species in our case. Our high Ag^+/Si–H molar ratio was necessary due to the intended antibacterial application.

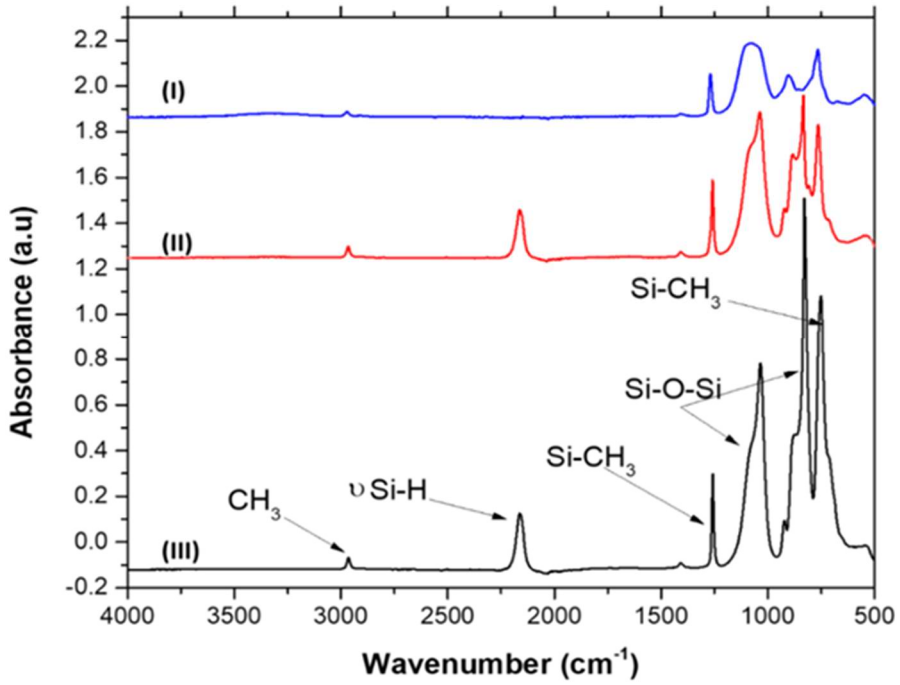

Figure 1. ATR-FTIR spectra of PMHS before and after reaction with $AgNO_3$ at different mole ratios: (I) (Ag^+/Si–H of 50:2); (II) (Ag^+/Si–H of 2:50); and (III) liquid PMHS

In addition to Ag, other metal nanoparticles, such as those of Au, Pt, Ta, and Nb can be synthesized by PMHS [31]. In fact, the active Si–H moiety arranged periodically on the siloxane backbone in the

PMHS matrix, provides intrinsic sites to synthesize and integrate these metal nanoclusters [20]. Ag-PMHS nanocomposites exhibit a surface plasmonic resonance phenomenon, which is similar to other chemical reduction syntheses of Ag-NPs. This surface plasmon resonance is due to the collective oscillation of conducting electrons of Ag-NPs, characteristically observed by a color change in Ag-PMHS solutions. Notably, when $AgNO_3$ is added to the PMHS gel, a redox reaction begins immediately with a color change from colorless to yellow, orange, brown, and black (nucleation, nanoparticles, nanoclusters, and growth of controlled aggregates, respectively), as well as, the corresponding formation of different Ag species [20]. In fact, it has been reported that using NH_3 (aq) as a catalyst, $Si^{\delta+}$–$H^{\delta-}$ bonds are polarized via the intermediate formation of hypercoordinated silicon species to increase the sol–gel reaction rate [32]. At the gel point (achieved after 24 h), a viscous, stable and elastic gel network was observed. Note that typical sol-gel process without NH_3 (aq) can last for ~1000 h[33]. In deed, the NH_3 (aq) does not only catalyze the hydrolysis process but also forms a complex ion with Ag^+ ($Ag(NH_3)_2^+$aq) to accelerate the reduction of Ag^+ ions by PMHS. This is similar to saccharides reduction of Ag^+ ions (in the presence of NH_3 (aq)) in a typical modified Tollens Ag synthesis[34-35]. However, for the purpose of obtaining a thin Ag-PMHS nanocomposite coating on AAO/Al, the ageing process was limited to 30 min in our experiment.

Figure 2 (A) shows the energy dispersive X-ray spectroscopy (EDS) spectrum of elements in the Ag–PMHS nanocomposite (Ag+/Si–H of 50:2 mole ratio), which comprises C, O, and Si with their respective K_α peaks at 0.28, 0.52, and 1.73 keV respectively, and an L_α peak of Ag at 2.98 keV. Similarly, the XRD pattern is shown in Figure 2 (B). The XRD pattern matched well with the JCPDS card (89-3722) standard data of Ag, characterized by a face-centered cubic crystalline

silver, with corresponding prominent peaks for 2θ at 38.17°, 44.31°, and 64.44 °. Both the EDS and XRD spectra confirm the formation of Ag-NPs in the PMHS siloxane polymer.

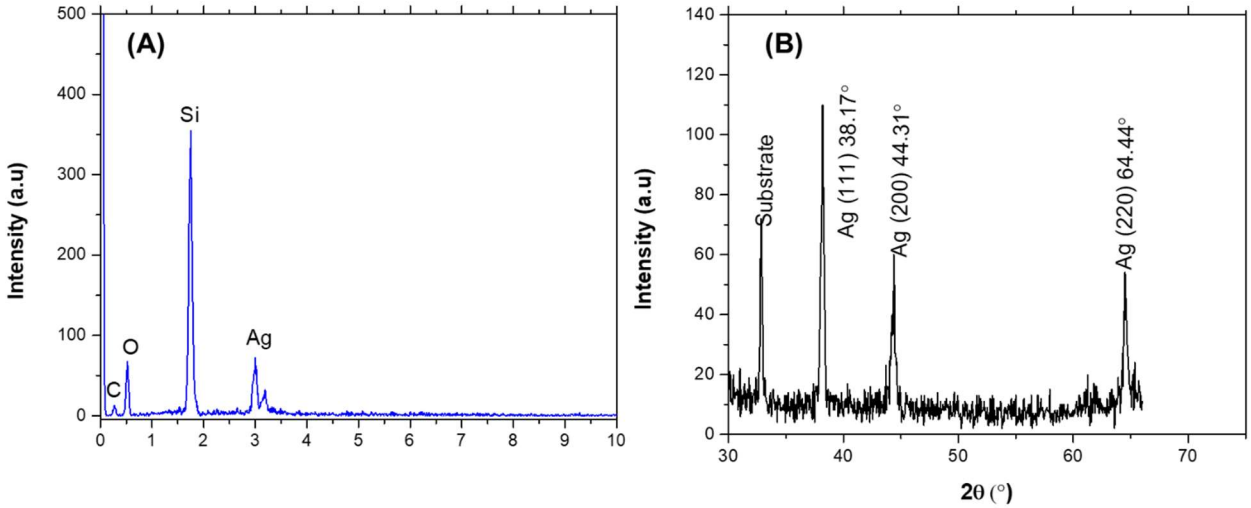

Figure 2. (A) EDS spectrum and (B) XRD pattern of as-synthesized Ag-PMHS nanocomposite having a Ag^{+}/Si–H molar ratio of 50:2.

Anodization. In the present study, anodization was performed to engineer an Al substrate to achieve a high surface topography for coating the Ag-PMHS nanocomposite. Anodization is ideal because it is technologically scalable and offers abrasion and corrosion resistance [36]. In a typical galvanostatic anodization process, potential increases linearly with anodization time [37]. The process begins with nucleation and the subsequent growth of porous structures (Figure 3 (A)). As oxide dissolution begins, porous structures are formed. Finally, a steady state of oxide dissolution and formation equilibrium is attained. Notably, for the 120 min sample, the potential increased linearly with time, and beyond the critical voltage (49 V) after 60 min of anodization (Figure 3 (B)). This rise was due to the high resistance of the oxide barrier layer. Beyond the critical voltage, the potential decreased marginally (a decrease of ~4 V) with anodization time, until the rate of oxide dissolution was equivalent to the rate of porous oxide layer formation [38]. However, for both

the 60 min and 30 min samples, incomplete anodization was observed. Hence, the 120 min anodized sample was selected for the remainder of the study.

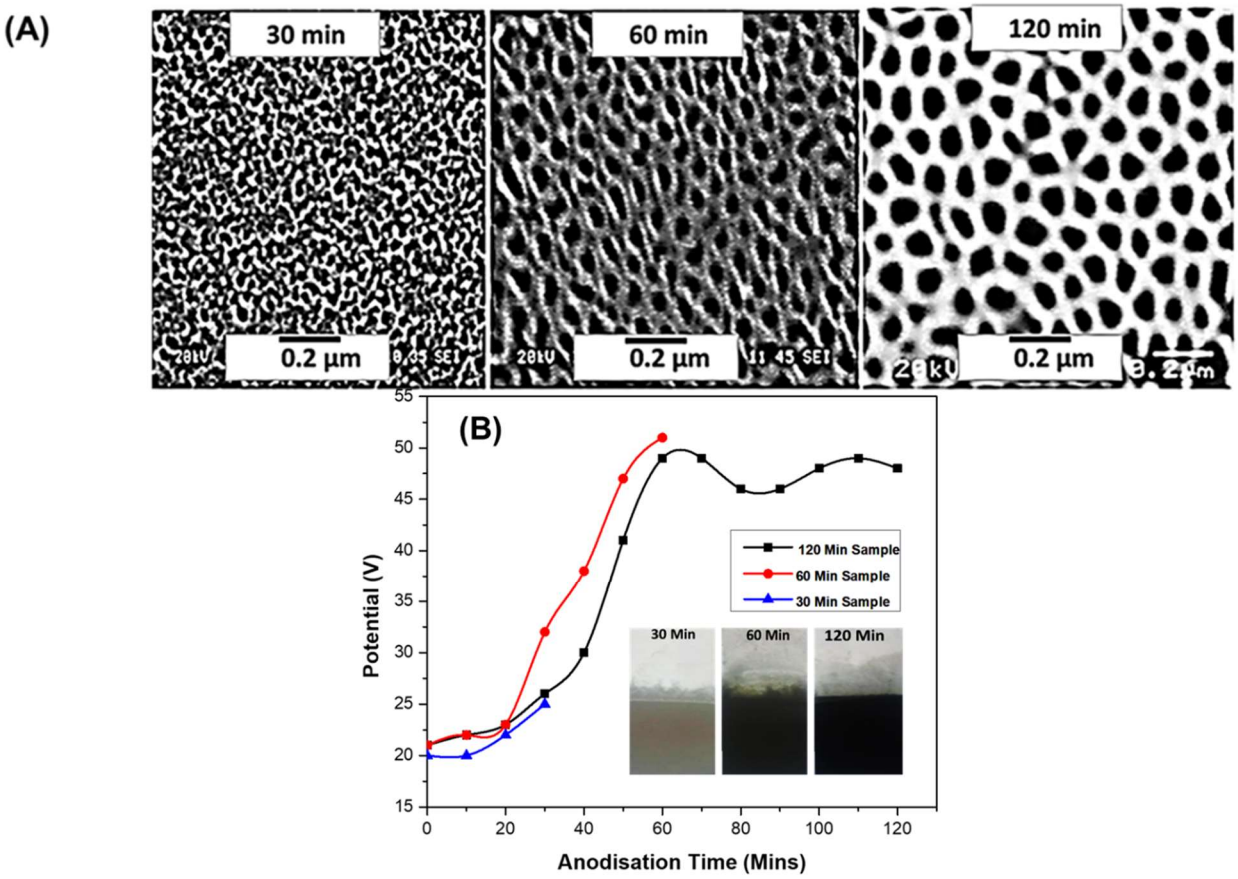

Figure 3 (A) SEM image of anodized aluminum oxide (AAO) after a 30 min anodization (left); 60 min (middle); and 120 min (right): (B) kinetics of anodization process for the three samples above (where ■ 120 min; ● 60 min; and ▲ 30 min). Inset: Digital image of the three samples.

To engineer a superhydrophobic Ag–PMHS nanocomposite coating on Al with inherent antibacterial property, the Ag–PMHS nanocomposite with a Ag^{+}/Si–H molar ratio of 50:2 was coated on the 120 min anodized Al (herein referred to as AgP–NcAAO) and used for the

remainder of the study. Both the XRD (Figure 4 (A)) and EDS spectra (Figure 4 (B)) show that the chemical composition of the fabricated AgP–NcAAO sample comprises Al and O; and Ag, Si, and C; from Al_2O_3 (owing to anodization) and the Ag–PMHS nanocomposites, respectively. The broad peak at 10.0° is typical for amorphous SiO_2 [39], which arises from the reaction of PMHS with $AgNO_3$. Notably, the Al peaks ((111), (200), (220), and (311) from the underlying Al substrate), overlap with the Ag peaks ((111), (200), (220), and (311)). The overlapping of diffraction peaks of Al (111) and Ag (111) is due to their similar lattice parameters (Figure 4 (A), inset). The presence of sulfur in the EDS spectra of Figure 4 (B) can be ascribed to sulfuric acid from anodization. It is noteworthy that an optimal wt.% RTV silicone was used to improve the adhesive bonding of the AgP–NcAAO sample (herein referred to as 04Sil-AgP–NcAAO) (Figure 4 (B (III)).

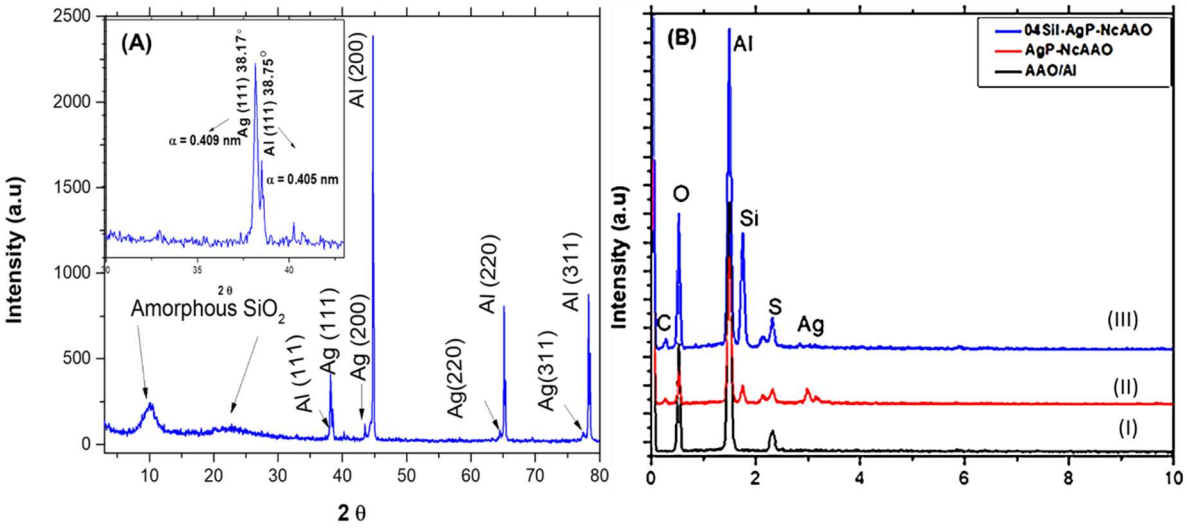

Figure 4: (A) XRD pattern of Ag–PMHS nanocomposite having a Ag^+/Si–H molar ratio of 50:2.0 coated on AAO/Al (AgP–NcAAO); (B) EDS spectra of : (I) AAO/Al; (II) AgP-NcAAO; (III) 0.4% w/v silicone incorporated in AgP–NcAAO

(04Sil-AgP–NcAAO). (Inset: high magnification of Ag and Al (111) planes with their lattice parameters)**.**

Superhydrophobic property. The two well-known conditions for fabricating superhydrophobic surfaces are the combined effects of low surface energy and geometrical surface structure[40]. In the present study, the desired topography was achieved through the combined effects of Al anodization and presence of silver nanoparticles (Ag-NPs), while low surface energy, by passivation with PMHS molecules. Though, two-step anodization process produces self-organised densely hexagonal AAO templates[41], the process is somehow complex and time consuming, hence we have deployed a one-step constant current hard anodisation process to achieve desired surface topography. The surface roughness and CA of the as-received Al substrate were 0.4 ± 0.02 μm and 94 ± 1.2°, respectively. CA of 113 ± 1.5° was observed for the Ag–PMHS nanocomposite coating on this surface (as shown in supplementary information, Table S1). Table 2 and Figure 5 provide information regarding the surface roughness and SEM micrograph. After a 120 min anodization, uniformly distributed nanopores of average pore diameter and cell diameter 60 ± 11 nm and 121 ± 19 nm, respectively, were observed (Table 3). The surface roughness and CA of 9.1 ± 0.9 μm and 8 ± 0.2°, respectively, were obtained for 120 min AAO (Figure 5 B). This shows that anodization affected the superhydrophilic property on the Al alloy surface. According to the Wenzel model [42], this is due to the increase wettability of the anodized surface. By contrast, the surface roughness of 9.7 ± 1.0 μm and CA of 159 ± 1.2° were achieved for the Ag–PMHS nanocomposite coating on the 120 min AAO sample (AgP–NcAAO) (Figure 5 C). The combined effects of the low surface energy PMHS and the empty space by micro-nanostructures, induced by both Ag-cluster and AAO lead to superhydrophobicity that can be explaind by Cassie-Baxter

model[43]. The change in surface wettability from superhydrophilic to superhydrophobic can be attributed to both the nano-micro surface roughness (induced by both Ag-NPs and anodization) and the presence of low surface-energy organosilicon (long Si–CH_3 chain). The presence of Ag-NPs, presumably increase the nano-micro roughness of the Ag-PMHS nanocomposite . We have observed a linear relationship between the CA of the coatings on AAO and Ag:PMHS molar ratio (supplementary information can be found in Table S1, describing contact angle measurements of Ag-PMHS nanocomposites at different molar ratio on Al substrates). However, in the absence of Ag-NPs, a lower CA of 123 ± 3.1° was obtained for PMHS coated on AAO. Indeed, we have shown in our previous contribution that a high water CA (~152°) could only be achieved after appropriate combination of PMHS molecule and nano-micro roughness, induced by colloidal TiO_2 NPs[28]. To improve the adhesive property of the AgP–NcAAO sample, RTV-silicone, a well-known adhesive and hydrophobic silicone copolymer with water CA < 120° [44], was loaded into the Ag–PMHS nanocomposites. Consequently, the CA increased to above 150° (Figure 5 D).

Table 2. The surface topography of samples

Samples	Surface Roughness (rms) /µm
As-received Al Alloy	0.4 ± 0.02
120 min AAO	9.1 ± 0.9
AgP-NcAAO	9.7 ± 1.0
04Sil-AgP-NcAAO	8.9 ± 2.0

Table 3 : Morphological features of anodized samples at varied anodization time

Samples	Pore Diameter: D_p (nm)	Cell Diameter: D_c (nm)	Wall Thickness: W (nm)	Oxide Thickness (µm)	Pore Density: n (Pore/cm^2)	Porosity: α (%)
120 min	60 ± 11	121 ± 19	31 ± 4	75 ± 2.0	7.9 x 10^9	22
60 min	39 ± 18	90 ± 20	26 ± 2	56 ± 1.0	1.4 x 10^{10}	39
30 min	26 ± 6	59 ± 14	17 ± 4	36 ± 0.7	3.3 x 10^{10}	40

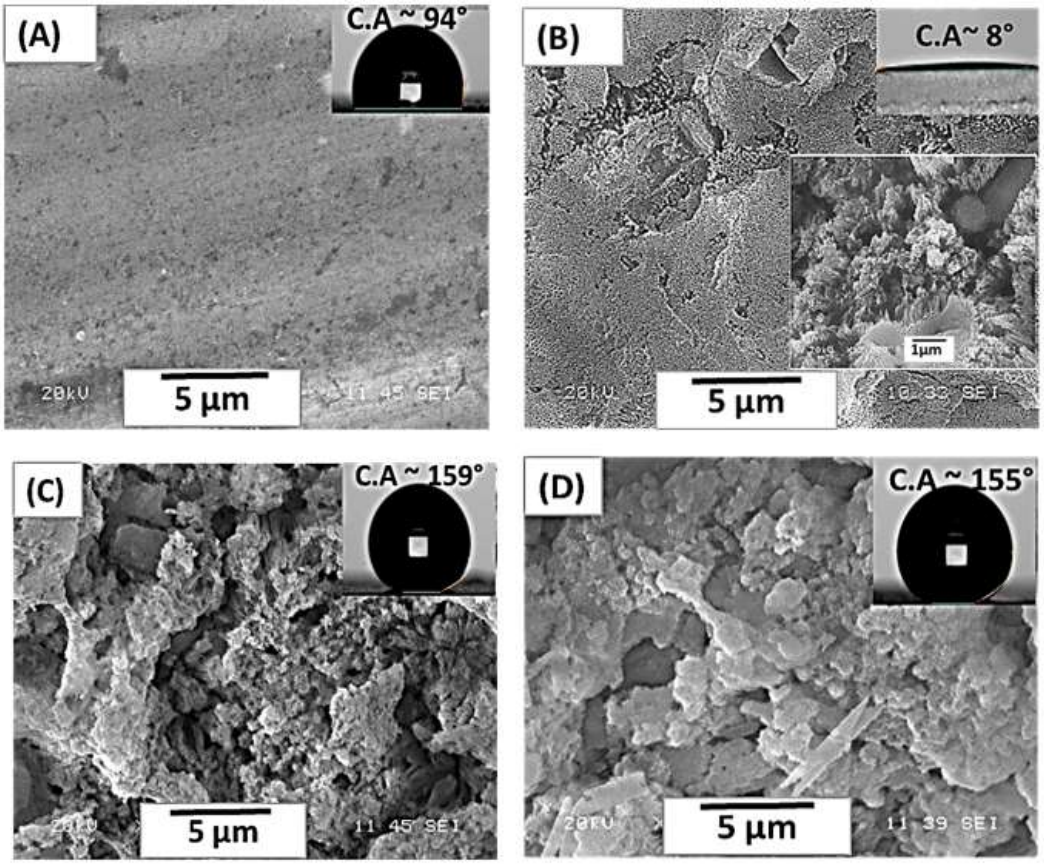

Figure 5. SEM images of (A) as-received Al; (B) AAO/Al; (C) Ag–PMHS nanocomposite having a Ag^+/Si-H molar ratio of 50:2 coated on AAO/Al (AgP–

NcAAO); (D) 0.4 % w/v silicone incorporated in AgP–NcAAO (04Sil-AgP–NcAAO); The insets show 5 µL water drops deposited on the surface along with 1 and 5 µm scale bars

In particular, we observed that after silicone loading, the CA increased from 8 ± 0.2° for 120 min AAO, to 155 ± 0.4 ° for 04Sil-AgP–NcAAO. Interestingly, increasing the silicone wt.% resulted in an 8° decrease in CA (Figure. 6). This trend is similar to our previous observation when silicone wt.% was deposited on etched Al [45]. The decrease in CA following the continuous silicone loading can be attributed to the filling-in of the AAO micro- and nanostructures, which results in the smoothening the rough surface. However, the AgP–NcAAO sample resulted in a higher surface roughness of 9.7 ± 1.0 µm and CA of 159 ± 0.5°, compared with surface roughness of 8.9 ± 2.0 µm and CA of 155 ± 0.4°, for the 04Sil-AgP–NcAAO sample. It must be re-emphasized that the high CA value for the AgP–NcAAO, relative to 04Sil-AgP–NcAAO, is attributed to the partial filling of the entrapped air in the micro–nanoporous structures by RTV-silicone, in accordance with the Cassie–Baxter model [43].

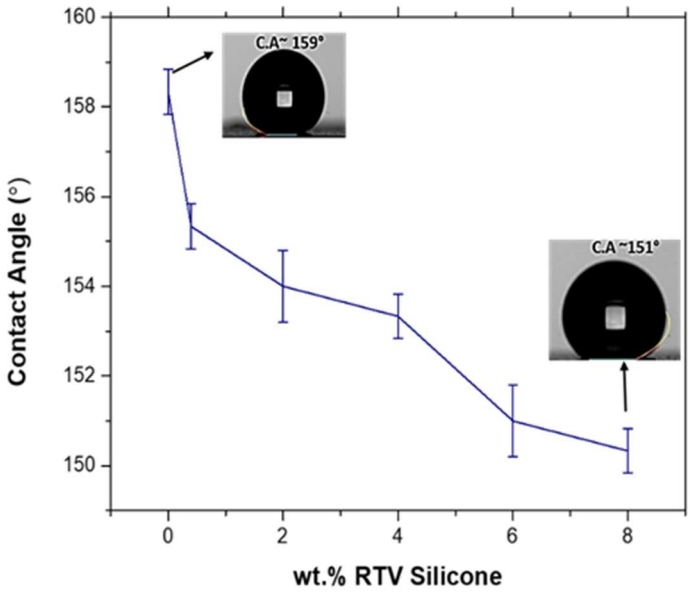

Figure 6. Water contact angle on the surface of Ag–PMHS nanocomposites having a Ag^{+}/Si–H molar ratio of 50:2 as a function of wt.% of incorporated silicone.

According to the Cassie–Baxter model, a rough surface would repel liquid droplets owing to the entrapped air in the nano- and/or microstructural features[43]. The anodization of Al, results in the formation of porous nano- and/or microstructural Al_2O_3 features. The OH group in Al_2O_3 can form a strong monodentate or bidentate bonding with the Si–O–Si group of Ag–PMHS. In particular, the silanol molecule replaces the OH group, resulting in the formation of water molecules and a strong a SiO−Al monodentate bonding on the Al_2O_3 surface[46]. Such a strong chemical bonding, coupled with AAO's ability to mechanically anchor PMHS, can increase the adhesion bonding of PMHS coatings.

Note that 0.4% (w/v) silicone was deemed optimal for adhesive bonding studies. A test was performed using the American Standard Test Method (ASTM D 3359-02) on four samples (Figure 7 and supplementary information, Table S2 A-D, show grade of adhesive bonding on tested samples). The Ag–PMHS nanocomposite coating on the as- received Al, exhibited the lowest grade of 0B, while the Ag–PMHS nanocomposite coating on AAO exhibited grades between 4B and 5B. Interestingly, after 90 days of saline immersion, the Ag–PMHS nanocomposite coating on AAO was still resistant to scratch (supplementary information can be found in Table S 2D, showing grade of adhesive bonding of Ag–PMHS nanocomposite coating on AAO after 90 days of saline immersion). According to ASTM D3359-02, coatings with 5B grade exhibit the highest adhesion bonding, whereas those with

grade 0B exhibit the lowest adhesion [47]. Notably, anodization provides an optimal surface topography that affords high abrasive resistance to Ag–PMHS nanocomposite coating. The high adhesive bonding observed can be attributed to both chemical and physical phenomena. Chemically, the RTV-silicone increases the monodentate bonding of the Si–O–Si group and the Al_2O_3. This is confirmed by the increased intensity of siloxane groups in the FTIR peaks of the 04Sil-AgP–NcAAO (as shown in supplementary information, figure S1(I)). Physically, anodization provides additional support for anchoring the Ag–PMHS nanocomposite coating. In fact, the 04Sil-AgP–NcAAO sample maintains the superhydrophobic property (More details can be found in Video S1, as a movie demonstration of water roll-off property of the superhydrophobic surface) albeit with a 4° decrease in CA with increased adhesion bonding; therefore, it is ideal for practical applications.

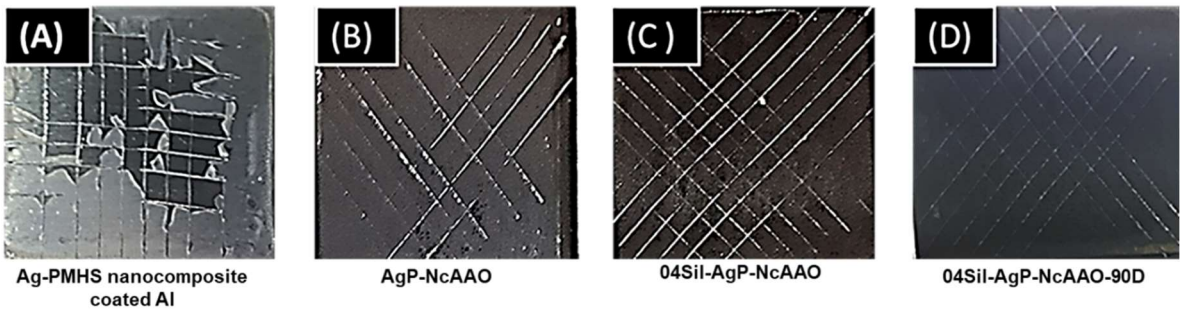

Figure 7. Digital images of scratch test based on American Standard Test Method (ASTM D 3359-02) showing the adhesion of Ag–PMHS nanocomposite coatings having a Ag^+/Si–H molar ratio of 50:2 on: (A) as-received Al; (B) AAO/Al (AgP-NcAAO); (C) 0.4 % w/v silicone incorporated in AgP–NcAAO (04Sil-AgP–NcAAO); and (D) 04Sil-AgP–NcAAO in 90 days of immersion (04Sil-AgP–NcAAO-90D).

Because the chemical nature of the Ag-NPs' surface is crucial for Ag^{+} release kinetics, a representative portion of the superhydrophobic AAO/Al sample (04Sil-AgP-NcAAO) was examined through EDS analysis for elemental mapping. Among three different locations of the elemental mapping, Figure 8 (A) shows the SEM micrograph of the representative sites, while Figures 8 (B, C, and D) show the elemental mapping of Ag, Al, and Si, respectively. Dispersed Ag is distributed on the entire area, as shown in Figure 8 (B). However, clusters of Ag are visible, as marked in the same figure. Conversely, Al surrounds Ag (dark region) in the Al mapping, as shown in Figure 8 (C). Figure 8 (D) shows that Si, from the PMHS molecules, is distributed uniformly across the entire sample. Therefore, the elemental mapping demonstrates that elemental Ag is distributed over the entire range of the randomly selected area.

.

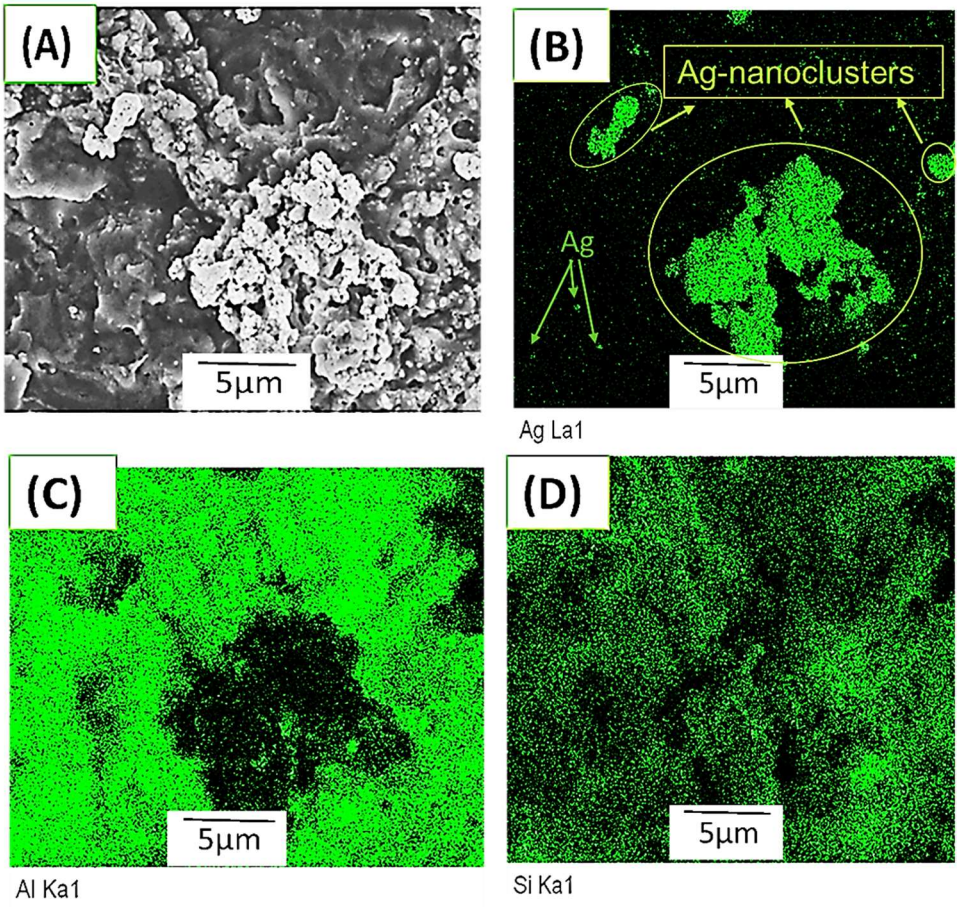

Figure 8. EDS mapping of 0.4% w/v silicone incorporated in Ag–PMHS nanocomposites having a Ag^{+}/Si–H molar ratio of 50:2 coated on AAO/Al(04Sil-AgP-NcAAO); (A) SEM image (B) Silver; (C) Al; and (D) Silicon.

Bacterial susceptibility study. Antibacterial study was performed using two methods. First, antibacterial activity of the Ag–PMHS nanocomposites by the Kirby Bauer disk diffusion assay; second, anti-biofouling study. As model microbes, S.A, P.A, and E-coli were used. It is noteworthy that these bacteria are among the 12 families of the most dangerous antibiotic-resistant bacteria or "superbugs," of clinical significance[48]. The Kirby Bauer assay utilizes the ZOI to describe regions

around the antimicrobial agent, where bacteria colony or growth is inhibited owing to the former's ability to diffuse. Figure 9 shows the results of the disk diffusion assay.

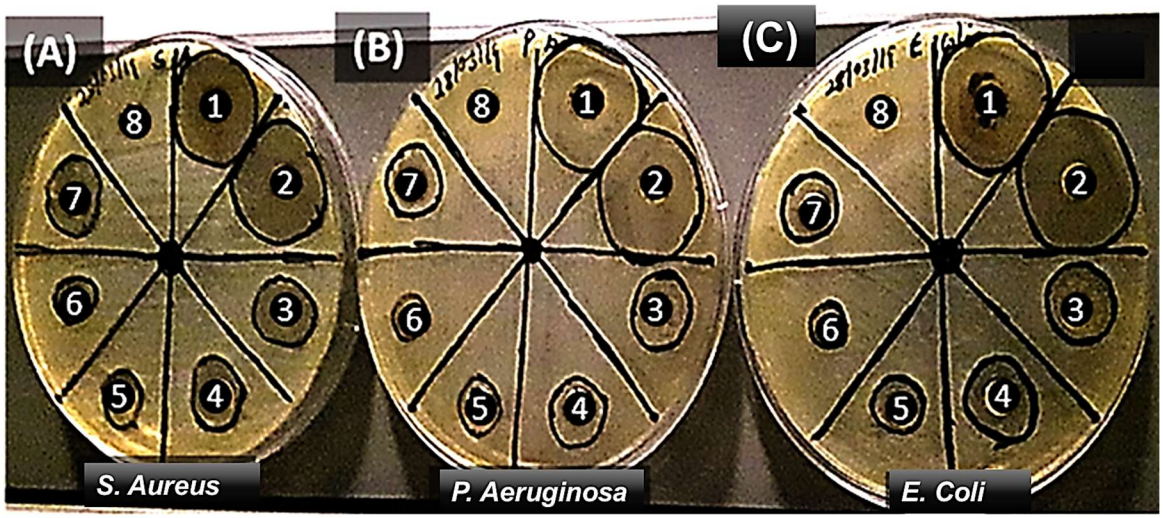

Figure 9. Antibacterial activity of Ag–PMHS nanocomposites against: (A) *Staphylococcus aureus* (S.Aureus); (B) *Pseudomonas aeruginosa* (P.A*eruginosa*); and (C) *Escherichia coli* (E-coli). Region 1 (Ag+/Si–H of 50:1); region 2 (Ag+/Si–H of 50:2); region 3 (Ag+/Si–H of 50:30); region 4 (Ag+/Si–H of 50: 40); region 5 (Ag+/Si–H of 50:50); region 6 (Ag+/Si–H of 2:50); region 7 (Ag+/Si–H of 1:50); region 8 represents the Control (mineral spirit + PMHS) (Disk diffusion assay, represents three independent experiments.

Notably, the Ag^{+}/Si–H molar ratio of 50:2 was the most effective, followed by 50:1, and the least being 2:50. The relatively high ZOI value for the Ag^{+}/Si-H molar ratio (1:50), may be due to the antibacterial and anti-biofouling synergistic effect. The mean and standard deviation values of the ZOI for S.A, P.A, and E-coli are 23.3 ± 3.6, 25.3 ± 0.5, and 24.8 ± 0.5 mm, respectively. These ZOI values are well within the acceptable range (8–30 mm) for standard antibiotics against S.A,

P.A, and E-coli, per the Clinical and Laboratory Standards Institute standards [49]. This shows that the Ag–PMHS nanocomposite at a higher Ag^+/Si–H molar ratio such as 50:2, is an effective antibacterial agent, particularly for gram negative bacteria compared with the gram-positive bacterium S.A. However, at a lower Ag^+/Si–H molar ratio such as 2:50, the Ag–PMHS nanocomposite was less effective at inhibiting all the bacteria, with ZOI values of 9.0 ± 0.8, 8.5 ± 0.6, and 6.8 ± 0.5 mm for S.A (gram +ve), P.A (gram - ve), and E-coli (gram -ve), respectively (Figure 10). This can be explained by the fact that as Ag-NPs are locked up at the Si–H reducing sites (Eq. 1), less Ag^+ ions effectively leach out to interact with bacteria to induce their lethal effects. Contrarily, at higher molar ratios of Ag^+/Si–H such as 50:2, excess amounts of Ag-NPs are available to leach out a high amount of Ag^+ ions to induce an increased antibacterial effect. The difference in bioactivity between the two classes of bacteria (gram-ve and gram+ve) may be ascribed to the difference in their cell wall composition and structure. Gram (+ve) bacteria have a thicker peptidoglycan layer composed of short peptides along with a linear polysaccharide chain cross-linking network. This rigid structure inhibits the penetration of Ag-NPs. By contrast, gram (-ve) bacteria have a relatively thinner peptidoglycan layer, overlaid with an outer lipid cell membrane.

Although the antibacterial mechanism of Ag-NPs is still a scientific debate, the generally held view is that, upon bacterial/Ag-NPs contact, Ag-NPs are oxidized into Ag^+ by respiratory enzymes [50]. It is the released Ag^+ ions that cause the biocidal effect [50]. The Ag^+ ion is electrostatically attracted to the negatively charged cell wall. In particular, the Ag^+ ion binds with the purine and pyrimidine base pairs, rapturing the H-bonds in the base pairs, which results in denaturing and Deoxyribonucleic acid (DNA) disruption[50]. Such Ag^+ ion-cell membrane interactions prevent

DNA replications [51] and subsequently lead to bacterial death [52]. Additionally, Ag-NPs can induce toxicity via reactive-oxygen-species (ROS) -mediated free radical release, which leads to oxidative stresses and possible bacterial death. Therefore, the PMHS molecule may offer a polymeric matrix for holding and presumably triggering controllable Ag^+ release to kill microorganisms via the oligodynamic effect. It should be noted that Ag^+ ion of concentrations, 1-10 ppm (commonly measured by Inductively coupled plasma mass spectrometry (ICP-MS)) are known to impact antibactial property without adverse effect on mammalian cell[53-55]. However, Ag^+ release kinetics and cytotoxic impact studies, for example on fibroblasts cell lines, are beyond the scope of current work and would be reported in our future contribution.

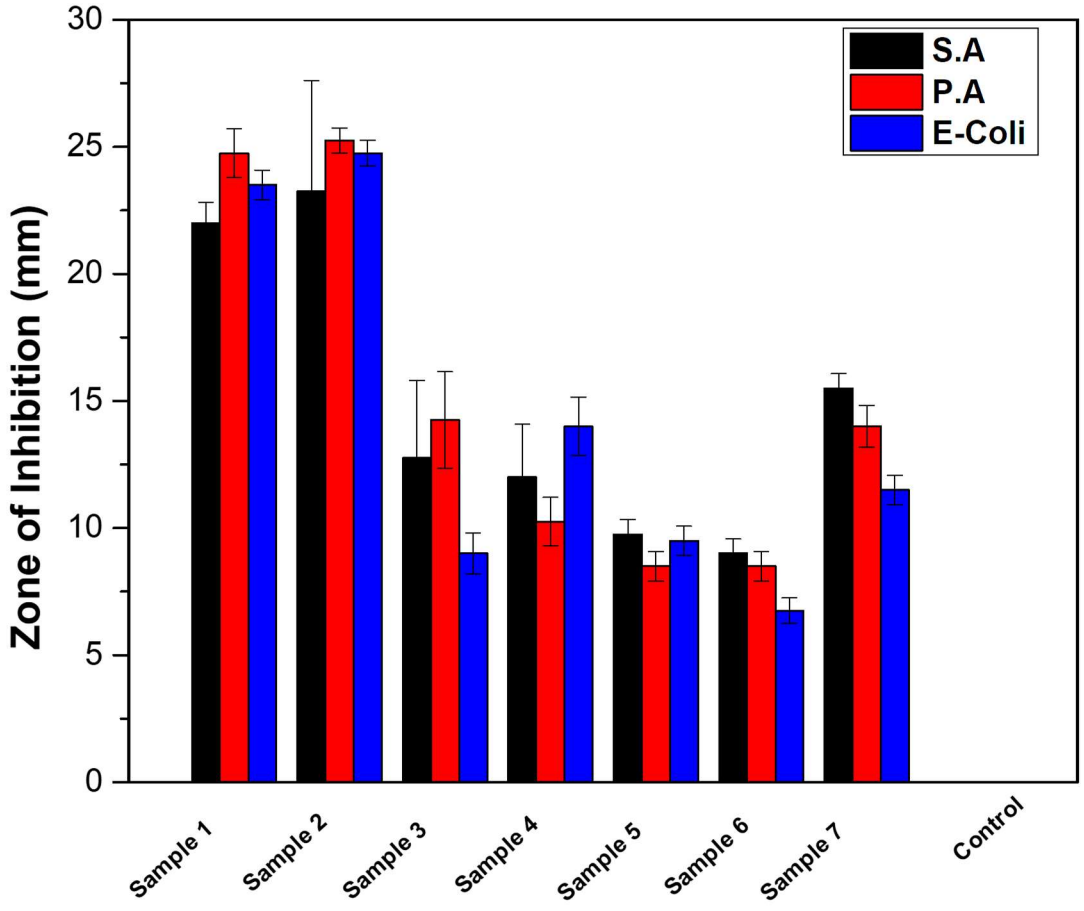

Figure 10. Graphical representation of zone of inhibition of Ag–PMHS nanocomposite against model bacteria. Sample 1 (Ag^+/Si–H of 50:1); sample 2 (Ag^+/Si–H of 50:2); sample 3 (Ag^+/Si–H of 50:30); sample 4 (Ag^+/Si–H of 50:40); sample 5 (Ag^+/Si–H of 50:50); sample 6 (Ag^+/Si–H of 2:50); sample 7 (Ag^+/Si–H of 1:50); Control (mineral spirit + PMHS). (Error bars represent SD (standard deviations), and data are from three independent experiments).

Anti-biofouling and biofilm inhibition assay: Bacterial adhesion reduction was performed by two methods. First, by anti-biofouling study; and second, by biofilm inhibition study. Note that limited incubation time was used for the anti-biofouling study. It appears water repellency of most of the superhydrophobic surfaces are lost over time, due to fragility of the surface micro/nano structures and fast surface chemistry degradation [56]. For example, the water roll-off property of a bioresin-based superhydrophobic coating was lost within 6-24 h, leading to colonization by P. A, S.A and E-coli bacteria. Similarly, gram (+ve) S.A cells completely colonized superhydrophobic titanium surface after 18 h incubation period[13]. By contrast, it seems reports on limited incubation time (30 min- 3 h), have demonstrated effectiveness of superhydrophobic coating at inhibiting bacterial attachment[23-25, 57-58].

Anti-biofouling performance was evaluated by determining the relative bacterial adhesion reduction using the following equation[59].

$$R\ (\%) = \left[\frac{(A-B)}{A}\right] \text{ x } 100 \qquad (5)$$

where R is the bacterial reduction (%), A the number of bacteria colonies/cm^2 on anodized Al substrate ((AAO/Al), used as control sample), and B the number of bacteria colonies/cm^2 on

superhydrophobic AAO/Al sample (04Sil-AgP–NcAAO) having CA of 155 ± 0.4°. It must be reiterated that the most promising sample (having Ag+/Si–H molar ratio of 50:2),which exhibited both superhydrophobic and high adhesive properties, was used as test sample for the anti-biofouling study. Such dual action superhydrophobic–biocide, is likely to possess excellent bacterial repellency and inhibits bacterial attachment, even after loss of superhydrophobicity. Figure 11 shows the graphical representation of bacterial adhesion/cm^2 reduction for the model bacteria of S.A, P.A, and E-coli. The number of S.A colonies on AAO/Al and the superhydrophobic AAO/Al sample (04Sil-AgP–NcAAO) were 6.5×10^7 and 4.5×10^5, respectively. It is worthy of note that bacteria colonies on the superhydrophobic AAO/Al sample (04Sil-AgP-NcAAO) are two orders less than those on the control sample surfaces (AAO/Al), representing a 2.2 log and 99.3 % S.A reduction. Similar trend was observed for both gram (-ve) P.A and E-coli bacteria. The number of P.A bacterium that colonized the control sample(AAO/Al), was 5.0×10^6, compared to 5.0×10^4, on superhydrophobic AAO/Al sample (04Sil-AgP-NcAAO). Representing a two order of magnitude lower, a 2 log reduction and 99.0 % P.A bacterium reduction. In the case of E- coli, 5.0×10^6 colonies were observed on control sample (AAO/Al), as against 2.5×10^4 bacterial colonies on the superhydrophobic AAO/Al sample (04Sil-AgP–NcAAO). Clearly, superhydrophobic AAO/Al sample (04Sil-AgP–NcAAO) was most effective at inhibiting E-coli colonies compared to the other bacteria, with a 2.3 log reduction factor and a 99.5 % adhesion reduction efficiency. However, it should be mentioned that less bacterial adhesion reduction are observed for non Ag-based superhydrophobic coatings. For example, in the work of Meier, M et al[23], superhydrophobic filamented silicone (having CA~ 164 ± 5°) exhibited E-coli bacterium adhesion reduction of 84 ± 5 %, under 3 h incubation, while superhydrophobic rod-like silicone (having CA~ 168 ± 4°) showed E-coli bacterium reduction of 79 ± 7 %, under same

condition. Similar trend was also observed for gram (+ve) *S. epidermidis*. Superhydrophobic filamented silicone, exhibited adhesion reduction of 95 ± 3 %,while superhydrophobic rod-like silicone showed a reduction of 88 ± 7 %[23]. In a related study by Crick. C.R., et al[24], superhydrophobic silicone elastomer (with CA~ 168°), resulted in 79 % and 58 % adhesion reduction for both gram (-ve) E-coli, and gram (+ve) S.A, respectively. Interestingly, in our case, the incorporation of Ag in the superhydrophobic surface that provided a CA of 155 ± 0.4°, showed bacterial reduction efficiency of 99.3 %, 99.0 % and 99.5 % for the S.A, P.A and E-coli bacteria respectively. However, while direct comparison of different reported results must be treated with caution, as differences may arise owing to experimental conditions, these results somehow corroborate our hypothesis that antibacterial Ag-NPs incorporated in superhydrophobic coatings, can enhance the over all effectiveness of bacterial adhesion reduction.

Note that gram (-ve) bacteria such as E-coli and P.A are ubiquitous pathogens in biofilms even on dry inanimate surfaces[60-62]. Therefore, evaluating the superhydrophobic AAO/Al sample (04Sil-AgP–NcAAO)'s ability to inhibit biofilm growth is essential. Consequently, SEM was utilized to study the biofilm formation [63]. It has been reported that biofilm maturation begins after 24 h of incubation[64], henced 48 h incubation time was utilized to evaluate biofilm growth. As shown in Figure 11 (inset), the entire surface area of AAO/Al (uncoated AAO) is covered by the biofilm. By contrast, the biofilm is not observed on the superhydrophobic AAO/Al sample (04Sil-AgP–NcAAO), except a few bacteria scattered over the surface.

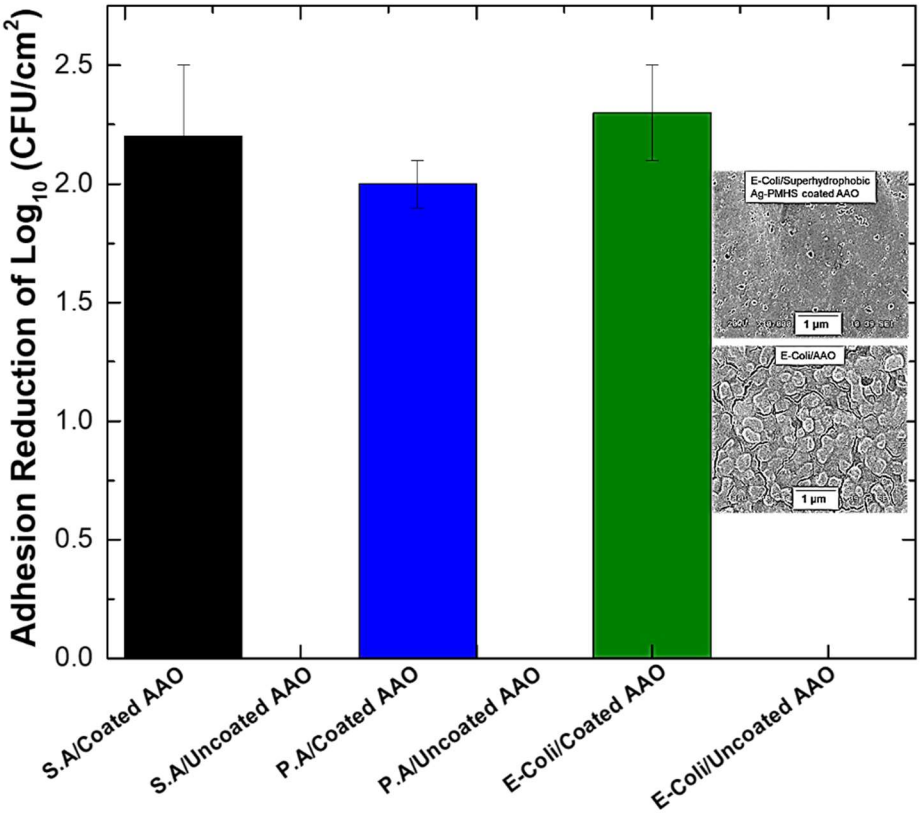

Figure. **11**: Adhesion reduction of bacteria (S.A, P.A, or E-coli) on superhydrophobic AAO/Al sample (04Sil-AgP–NcAAO); and control sample (AAO/Al). Data represent multiple independent experiments. Inset: SEM micrograph of E-coli biofilm on superhydrophobic AAO/Al sample (Top); and control sample (AAO/Al) (Bottom).

It is noteworthy that the superhydrophobic AAO/Al sample (04Sil-AgP–NcAAO) lost its water roll-off property after 3 h of being in contact with bacteria. The complex mechanism for bacterial attachment on superhydrophobic coatings, comprising cell adhesion, Van der Waals interactions and activation of quorum sensing molecules, are well acknowledged[65]. This necessitates the need

for further detailed studies to establish the correlations between bacteria type, surface chemistry and surface morphology[66]. Nevertheless, it is very likely, bacteria in contact with Ag–PMHS nanocomposites release bacterial secretions (biopolymers, ß lactamases, and other enzymes) [47] composed of hydrophilic ligands and proteins (N–H, O–H, and C=O) that alter the surface chemistry of the superhydrophobic AAO/Al sample (04Sil-AgP–NcAAO). Interestingly, the sample regained its water roll-off property (with an average CA of 155 ± 5.0°) after 3 days of air exposure, presumably due to the evaporation of the hydrophilic ligands. It is likely that 04Sil-AgP–NcAAO exists in the Wenzel wetting state at a high hydrophilic ligand concentration but in the Cassie-Baxter wetting state at a lower hydrophilic ligand concentration. Therefore, the bacterial adhesion reduction observed on superhydrophobic AAO/Al sample, may presumably be facilitated by leachable Ag^+ ions during the Wenzel state. However, for frequently touched surface applications, where the evaporation of the hydrophilic ligand is possible owing to excess dry air, the Cassie–Baxter state can be re-established to facilitate superhydrophocity. Note that PMHS coated on 120 min anodized Al exhibited a lower water CA of 123 ± 3.1°. Therefore bacterial adhesion reduction study was not performed. Such study would be explored in our future contribution.

To further explore the stability of the superhydrophobic sample, a 3-month saline water (3.5 wt.% NaCl, pH = 7.4) immersion study was performed. As shown in Figure 12, the CA was well above 150° after 90 days of saline water immersion. This signifies that the coating has a long-lasting stability in a physiological solution (pH 7.4), typically found in mammalia cells.

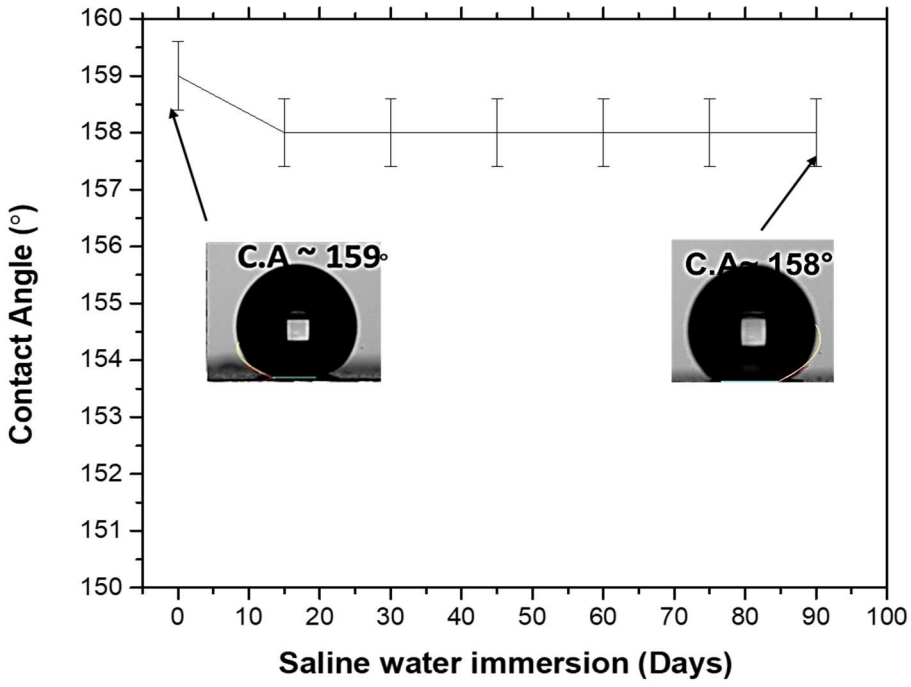

Figure 12. Water contact angle of the superhydrophobic sample with time of immersion in 3.5 wt.% NaCl solutions. CA was measured after drying samples for 2 h at 55 °C.

In general, the superhydrophobic sample exhibits both bactericidal and anti-biofouling properties. The bactericidal effect is observed owing to the possible release of Ag^{+} ions that electrostatically interact with the negatively charged cell wall of bacteria, to inactivate it. The anti-biofouling effect is achieved owing to the superhydrophobic property, induced by the combined effects of nano-micro roughness (achieved by Ag-NPs and anodization) and the presence of $–CH_3$ ligand from PMHS. Due to the superhydrophobicity, water has a minimum contact area with the surface, hence a weaker bacterial interaction would be expected on such surfaces. Therefore, it would be favorable

for bacteria to remain in solution and roll off the surface when tilted rather than adhere to the superhydrophobic surface [67].

CONCLUSIONS

In this study, a simple two-step approach was deployed to fabricate Ag–PMHS nanocomposite coatings on anodized Al. The as-synthesized Ag–PMHS nanocomposite coating demonstrated excellent antimicrobial properties against clinically relevant planktonic bacteria, with ZOI values of 25.3 ± 0.5, 24.8 ± 0.5, and 23.3 ± 3.6 mm for P.A, E-coli, and *S*.A, respectively. The Ag–PMHS nanocomposite coating exhibited a water CA of 159 ± 0.5°, providing an excellent anti-biofouling property with bacterial adhesion reductions of 99.0 %, 99.5 %, and 99.3 % for P.A, E-coli, and S.A, respectively. Stability study demonstrated a stable water CA of 158° after 90 days of immersion in saline water (3.5 wt.% NaCl, pH = 7.4). Remarkably, the superhydrophobic Ag–PMHS nanocomposite coating on anodized Al exhibited excellent scratch resistance and strong adhesion property. Overall, Ag–PMHS nanocomposite coating on anodized Al provides a promising and excellent candidate for potential use as antimicrobial touch surfaces to reduce the prevalence of nosocomial infections.

AUTHOR INFORMATION

Corresponding Author

*Corresponding author: dilip_sarkar@uqac.ca

The authors declare no competing financial interest.

ACKNOWLEDGMENTS

We acknowledge the financial support from Fonds de recherche du Québec - Nature et technologies (FRQNT) under the grant number 2018-LU-210883.

Supporting Information

Table of Content:

Figure S1: ATR- FTIR spectra of Ag-PMHS nanocomposite having a molar ratio of Ag^{+}/Si-H of 50:2.0 coated on AAO/Al (AgP-NcAAO); and 0.4 % w/v silicone incorporated in AgP-NcAAO (04Sil-AgP-NcAAO) respectively. The increased intensity of siloxane groups in the FTIR peaks for 04Sil-AgP–NcAAO compared to AgP-NcAAO signify the role of RTV siloxane in increasing the monodentate bonding between the Si–O–Si group and the AAO/Al.

Table S1: Contact angle measurements of Ag-PMHS nanocomposites at different molar ratio on various Al substrates. Contact angle of the coatings on AAO increased linearly with increasing Ag:PMHS molar ratio.

Table S2: Grade of adhesive bonding on tested samples. The Ag–PMHS nanocomposite coating on the as- received Al, exhibited the lowest grade of 0B, while the Ag–PMHS nanocomposite coating on AAO exhibited grades between 4B and 5B. Interestingly, after 90 days of saline immersion, the Ag–PMHS nanocomposite coating on AAO (Table S 2D) was still resistant to scratch with adhesive bonding Grade 5B.

Video S1: Demonstration of water roll-off property of superhydrophobic AAO/Al sample (04Sil-AgP-NcAAO). The AgP-NcAAO mantains its superhydrophobic property even after loading with 0.4 % w/v RTV silicone (04Sil-AgP-NcAAO).

REFERENCES

1. O'Toole, G.; Kaplan, H. B.; Kolter, R., Biofilm formation as microbial development. *Annual Reviews in Microbiology* **2000,** *54* (1), 49-79.
2. Hasan, J.; Hasan, J.; Crawford, R. J.; Ivanova, E. P., Antibacterial surfaces: the quest for a new generation of biomaterials. *Trends in biotechnology* **2013,** *31* (5), 295-304.
3. Taunk, A.; Chen, R.; Iskander, G.; Ho, K. K. K.; Black, D.; Willcox, M.; Kumar, N., Dual-Action Biomaterial Surfaces with Quorum Sensing Inhibitor and Nitric Oxide To Reduce Bacterial Colonization. *Acs Biomaterials Science & Engineering* **2018,** *4* (12), 4174-4182.
4. Algburi, A.; Comito, N.; Kashtanov, D.; Dicks, L. M.; Chikindas, M. L., Control of biofilm formation: antibiotics and beyond. *Appl. Environ. Microbiol.* **2017,** *83* (3), e02508-16.
5. Rabih, O. D., Device-Associated Infections: A Macroproblem That Starts with Microadherence. *Clinical Infectious Diseases* **2001,** *33* (9), 1567-1572.
6. Fair, R. J.; Tor, Y., Antibiotics and bacterial resistance in the 21st century. *Perspectives in medicinal chemistry* **2014,** *6*, PMC. S14459.
7. Awan, A. B.; Schiebel, J.; Böhm, A.; Nitschke, J.; Sarwar, Y.; Schierack, P.; Ali, A., Association of biofilm formation and cytotoxic potential with multidrug resistance in clinical isolates of Pseudomonas aeruginosa. *EXCLI journal* **2019,** *18*, 79.
8. Alexander, S.; Eastoe, J.; Lord, A. M.; Guittard, F. d. r.; Barron, A. R., Branched hydrocarbon low surface energy materials for superhydrophobic nanoparticle derived surfaces. *ACS applied materials & interfaces* **2015,** *8* (1), 660-666.
9. Han, K.; Park, T. Y.; Yong, K.; Cha, H. J., Combinational Biomimicking of Lotus Leaf, Mussel, and Sandcastle Worm for Robust Superhydrophobic Surfaces with Biomedical Multifunctionality: Antithrombotic, Antibiofouling, and Tissue Closure Capabilities. *ACS applied materials & interfaces* **2019,** *11* (10), 9777-9785.
10. Morán, M. C.; Ruano, G.; Cirisano, F.; Ferrari, M., Mammalian cell viability on hydrophobic and superhydrophobic fabrics. *Materials Science and Engineering: C* **2019,** *99*, 241-247.
11. Sousa, C.; Rodrigues, D.; Oliveira, R.; Song, W.; Mano, J. F.; Azeredo, J., Superhydrophobic poly (L-lactic acid) surface as potential bacterial colonization substrate. *AMB express* **2011,** *1* (1), 34.
12. Ellinas, K.; Tserepi, A.; Gogolides, E., Durable superhydrophobic and superamphiphobic polymeric surfaces and their applications: A review. *Advances in colloid and interface science* **2017,** *250*, 132-157.
13. Fadeeva, E.; Truong, V. K.; Stiesch, M.; Chichkov, B. N.; Crawford, R. J.; Wang, J.; Ivanova, E. P., Bacterial retention on superhydrophobic titanium surfaces fabricated by femtosecond laser ablation. *Langmuir* **2011,** *27* (6), 3012-3019.
14. Papadopoulos, P.; Mammen, L.; Deng, X.; Vollmer, D.; Butt, H.-J., How superhydrophobicity breaks down. *Proceedings of the National Academy of Sciences* **2013,** *110* (9), 3254-3258.

15. Zhang, M.; Wang, P.; Sun, H.; Wang, Z., Superhydrophobic surface with hierarchical architecture and bimetallic composition for enhanced antibacterial activity. *ACS applied materials & interfaces* **2014,** *6* (24), 22108-22115.
16. Heinonen, S.; Huttunen-Saarivirta, E.; Nikkanen, J.-P.; Raulio, M.; Priha, O.; Laakso, J.; Storgårds, E.; Levänen, E., Antibacterial properties and chemical stability of superhydrophobic silver-containing surface produced by sol–gel route. *Colloids and Surfaces A: Physicochemical and Engineering Aspects* **2014,** *453*, 149-161.
17. Wang, Z.; Ou, J.; Wang, Y.; Xue, M.; Wang, F.; Pan, B.; Li, C.; Li, W., Anti-bacterial superhydrophobic silver on diverse substrates based on the mussel-inspired polydopamine. *Surface and Coatings Technology* **2015,** *280*, 378-383.
18. Ozkan, E.; Crick, C. C.; Taylor, A.; Allan, E.; Parkin, I. P., Copper-based water repellent and antibacterial coatings by aerosol assisted chemical vapour deposition. *Chemical science* **2016,** *7* (8), 5126-5131.
19. Xiao, Z.-Y.; Huang, S.-X.; Zhai, S.-R.; Zhai, B.; Zhang, F.; An, Q.-D., PMHS-reduced fabrication of hollow Ag–SiO 2 composite spheres with developed porosity. *Journal of Sol-Gel Science and Technology* **2015,** *75* (1), 82-89.
20. Dag, O.; Henderson, E. J.; Wang, W.; Lofgreen, J. E.; Petrov, S.; Brodersen, P. M.; Ozin, G. A., Spatially Confined Redox Chemistry in Periodic Mesoporous Hydridosilica–Nanosilver Grown in Reducing Nanopores. *Journal of the American Chemical Society* **2011,** *133* (43), 17454-17462.
21. Zhai, S.-R.; Shao, X.; Zhou, D.; Zhai, B.; An, Q.-D., Sol–gel synthesis of nanosilver embedded hybrid materials using combined organosilica precursors. *Journal of sol-gel science and technology* **2012,** *62* (3), 281-286.
22. Shao, X.; Zhai, S.-R.; Zhai, B.; An, Q.-D., Ag+/MPTMS/PMHS-mediated two-step acid–base synthesis of hybrid materials with embedded nanosilver. *Journal of sol-gel science and technology* **2013,** *66* (2), 264-273.
23. Meier, M.; Dubois, V.; Seeger, S., Reduced bacterial colonisation on surfaces coated with silicone nanostructures. *Applied Surface Science* **2018,** *459*, 505-511.
24. Crick, C. R.; Ismail, S.; Pratten, J.; Parkin, I. P., An investigation into bacterial attachment to an elastomeric superhydrophobic surface prepared via aerosol assisted deposition. *Thin Solid Films* **2011,** *519* (11), 3722-3727.
25. Privett, B. J.; Youn, J.; Hong, S. A.; Lee, J.; Han, J.; Shin, J. H.; Schoenfisch, M. H., Antibacterial fluorinated silica colloid superhydrophobic surfaces. *Langmuir* **2011,** *27* (15), 9597-9601.
26. Bahrami, A.; Mokarram, R. R.; Khiabani, M. S.; Ghanbarzadeh, B.; Salehi, R., Physico-mechanical and antimicrobial properties of tragacanth/hydroxypropyl methylcellulose/beeswax edible films reinforced with silver nanoparticles. *International journal of biological macromolecules* **2019,** *129*, 1103-1112.
27. Siddaramanna, A.; Saleema, N.; Sarkar, D., A versatile cost-effective and one step process to engineer ZnO superhydrophobic surfaces on Al substrate. *Applied Surface Science* **2014,** *311*, 182-188.
28. Xiong, J.; Sarkar, D. K.; Chen, X. G., Ultraviolet-Durable Superhydrophobic Nanocomposite Thin Films Based on Cobalt Stearate-Coated TiO2 Nanoparticles Combined with Polymethylhydrosiloxane. *ACS Omega* **2017,** *2* (11), 8198-8204.
29. Zhang, J.; Hu, X.; Zhang, J.; Cui, Y.; Yuan, C.; Ge, H.; Chen, Y.; Wu, W.; Xia, Q., A fast thermal-curing nanoimprint resist based on cationic polymerizable epoxysiloxane. *Nanoscale research letters* **2012,** *7* (1), 380.
30. Sarkar, D.; Brassard, D.; El Khakani, M.; Ouellet, L., Dielectric properties of sol–gel derived high-k titanium silicate thin films. *Thin Solid Films* **2007,** *515* (11), 4788-4793.
31. Scheschkewitz, D.; Böhme, U., *Functional molecular silicon compounds*. Springer: 2014.

32. Corriu, R. J.; Lanneau, G. F.; Perrot-Petta, M.; Nehta, V. D., A new and mild access to N-functionalized formamido and thioformamido compounds using hypervalent silicon hydrides. *Tetrahedron Letters* **1990,** *31* (18), 2585-2588.
33. Pope, E.; Mackenzie, J., Sol-gel processing of silica: II. The role of the catalyst. *Journal of non-crystalline solids* **1986,** *87* (1-2), 185-198.
34. Sharma, V. K.; Yngard, R. A.; Lin, Y., Silver nanoparticles: green synthesis and their antimicrobial activities. *Advances in colloid and interface science* **2009,** *145* (1-2), 83-96.
35. Santipanusopon, S.; Riyajan, S.-A., Effect of field natural rubber latex with different ammonia contents and storage period on physical properties of latex concentrate, stability of skim latex and dipped film. *Physics Procedia* **2009,** *2* (1), 127-134.
36. Momen, G.; Farzaneh, M.; Jafari, R., Wettability behaviour of RTV silicone rubber coated on nanostructured aluminium surface. *Applied Surface Science* **2011,** *257* (15), 6489-6493.
37. Alkire, R. C.; Gogotsi, Y.; Simon, P., *Nanostructured materials in electrochemistry*. John Wiley & Sons: 2008.
38. Kikuchi, T.; Takenaga, A.; Natsui, S.; Suzuki, R. O., Advanced hard anodic alumina coatings via etidronic acid anodizing. *Surface and Coatings Technology* **2017,** *326*, 72-78.
39. Liou, T.-H.; Chang, F.-W.; Lo, J.-J., Pyrolysis kinetics of acid-leached rice husk. *Industrial & engineering chemistry research* **1997,** *36* (3), 568-573.
40. Brassard, J.-D.; Sarkar, D. K.; Perron, J., Synthesis of monodisperse fluorinated silica nanoparticles and their superhydrophobic thin films. *ACS applied materials & interfaces* **2011,** *3* (9), 3583-3588.
41. Masuda, H.; Masuda, H.; Fukuda, K., Ordered metal nanohole arrays made by a two-step replication of honeycomb structures of anodic alumina. *Science (New York, N.Y.)* **1995,** *268* (5216), 1466-1468.
42. Wenzel, R. N., Resistance of solid surfaces to wetting by water. *Industrial & Engineering Chemistry* **1936,** *28* (8), 988-994.
43. Cassie, A.; Baxter, S., Wettability of porous surfaces. *Transactions of the Faraday society* **1944,** *40*, 546-551.
44. Li, J.; Fan, L.; Wong, C.-P.; Lambert, F. C., Insulator coating and method for forming same. Google Patents: 2010.
45. Brassard, J.-D.; Laforte, J.-L.; Blackburn, C.; Perron, J.; Sarkar, D., Silicone based superhydrophobic coating efficient to reduce ice adhesion and accumulation on aluminum under offshore arctic conditions. *Ocean Engineering* **2017,** *144*, 135-141.
46. Poberžnik, M.; Kokalj, A., Implausibility of bidentate bonding of the silanol headgroup to oxidized aluminum surfaces. *Applied Surface Science* **2019,** *492*, 909-918.
47. Milionis, A.; Loth, E.; Bayer, I. S., Recent advances in the mechanical durability of superhydrophobic materials. *Advances in colloid and interface science* **2016,** *229*, 57-79.
48. Ho, P. L.; Ong, H. K.; Teo, J.; Ow, D. S.-W.; Chao, S. H., HEXIM1 peptide exhibits antimicrobial activity against antibiotic resistant bacteria through guidance of cell penetrating peptide. *Frontiers in microbiology* **2019,** *10*, 203.
49. Wayne, P., Clinical and laboratory standards institute. Performance standards for antimicrobial susceptibility testing. **2011**.
50. Banerjee, S. L.; Potluri, P.; Singha, N. K., Antimicrobial cotton fibre coated with UV cured colloidal natural rubber latex: A sustainable material. *Colloids and Surfaces A: Physicochemical and Engineering Aspects* **2019,** *566*, 176-187.
51. Zheng, K.; Setyawati, M. I.; Leong, D. T.; Xie, J., Antimicrobial silver nanomaterials. *Coordination Chemistry Reviews* **2018,** *357*, 1-17.
52. Percival, S. L.; Salisbury, A.-M.; Chen, R., Silver, biofilms and wounds: resistance revisited. *Critical reviews in microbiology* **2019**, 1-15.

53. Sikder, P.; Bhaduri, S. B.; Ong, J. L.; Guda, T., Silver (Ag) doped magnesium phosphate microplatelets as next-generation antibacterial orthopedic biomaterials. *Journal of Biomedical Materials Research Part B: Applied Biomaterials* **2020,** *108* (3), 976-989.
54. Menagen, B.; Pedahzur, R.; Avnir, D., Sustained release from a metal-Analgesics entrapped within biocidal silver. *Scientific reports* **2017,** *7* (1), 1-11.
55. Wei, L.; Lu, J.; Xu, H.; Patel, A.; Chen, Z.-S.; Chen, G., Silver nanoparticles: synthesis, properties, and therapeutic applications. *Drug discovery today* **2015,** *20* (5), 595-601.
56. Zhang, X.; Wang, L.; Levänen, E., Superhydrophobic surfaces for the reduction of bacterial adhesion. *Rsc Advances* **2013,** *3* (30), 12003-12020.
57. Hasan, J.; Webb, H. K.; Truong, V. K.; Pogodin, S.; Baulin, V. A.; Watson, G. S.; Watson, J. A.; Crawford, R. J.; Ivanova, E. P., Selective bactericidal activity of nanopatterned superhydrophobic cicada Psaltoda claripennis wing surfaces. *Applied microbiology and biotechnology* **2013,** *97* (20), 9257-9262.
58. Hizal, F.; Rungraeng, N.; Lee, J.; Jun, S.; Busscher, H. J.; Van Der Mei, H. C.; Choi, C.-H., Nanoengineered superhydrophobic surfaces of aluminum with extremely low bacterial adhesivity. *ACS applied materials & interfaces* **2017,** *9* (13), 12118-12129.
59. Cho, E.; Kim, S. H.; Kim, M.; Park, J.-S.; Lee, S.-J., Super-hydrophobic and antimicrobial properties of Ag-PPFC nanocomposite thin films fabricated using a ternary carbon nanotube-Ag-PTFE composite sputtering target. *Surface and Coatings Technology* **2019,** *370*, 18-23.
60. Sambhy, V.; MacBride, M. M.; Peterson, B. R.; Sen, A., Silver bromide nanoparticle/polymer composites: dual action tunable antimicrobial materials. *Journal of the American Chemical Society* **2006,** *128* (30), 9798-9808.
61. Bhatta, D. R.; Hamal, D.; Shrestha, R.; Subramanya, S. H.; Baral, N.; Singh, R. K.; Nayak, N.; Gokhale, S., Bacterial contamination of frequently touched objects in a tertiary care hospital of Pokhara, Nepal: how safe are our hands? *Antimicrobial Resistance & Infection Control* **2018,** *7* (1), 97.
62. Russotto, V.; Cortegiani, A.; Fasciana, T.; Iozzo, P.; Raineri, S. M.; Gregoretti, C.; Giammanco, A.; Giarratano, A., What healthcare workers should know about environmental bacterial contamination in the intensive care unit. *BioMed research international* **2017, 7,** ID. 6905450.
63. Ramage, G.; Walle, K. V.; Wickes, B. L.; López-Ribot, J. L., Biofilm formation by Candida dubliniensis. *Journal of clinical microbiology* **2001,** *39* (9), 3234-3240.
64. Loo, C.-Y.; Young, P. M.; Lee, W.-H.; Cavaliere, R.; Whitchurch, C. B.; Rohanizadeh, R., Superhydrophobic, nanotextured polyvinyl chloride films for delaying Pseudomonas aeruginosa attachment to intubation tubes and medical plastics. *Acta biomaterialia* **2012,** *8* (5), 1881-1890.
65. Naderizadeh, S.; Dante, S.; Picone, P.; Di Carlo, M.; Carzino, R.; Athanassiou, A.; Bayer, I. S., Bioresin-based Superhydrophobic Coatings with Reduced Bacterial Adhesion. *Journal of Colloid and Interface Science* **2020**, 574, 20-32.
66. Naderizadeh, S.; Dante, S.; Picone, P.; Di Carlo, M.; Carzino, R.; Athanassiou, A.; Bayer, I. S., Bioresin-based superhydrophobic coatings with reduced bacterial adhesion. *Journal of Colloid and Interface Science* **2020,** *574*, 20-32.
67. Freschauf, L. R.; McLane, J.; Sharma, H.; Khine, M., Shrink-induced superhydrophobic and antibacterial surfaces in consumer plastics. *PLoS One* **2012,** *7* (8), e40987.